Presented at Lake Louise Winter Institute: From Particles To The Universe, 2/20/2000-2/26/2000, Alberta, Canada

SLAC-PUB-11124

INITIAL PERFORMANCE OF THE BABAR EXPERIMENT

OWEN R. LONG (FOR THE BABAR COLLABORATION)
University of California, Santa Barbara, CA 93105, USA
E-mail: owen@slac.stanford.edu

We present the initial performance of the BaBar Experiment, as of April 2000. The PEP-II machine has reached a peak instantaneous luminosity of 1.95×10^{33} cm^{-2} s^{-1} and delivered an integrated luminosity of 7 fb^{-1} in the first 11 months of operation, of which 6.5 fb^{-1} has been logged by the BaBar experiment. This large data set has allowed us to study the performance of our detector in great detail and develop our physics analysis tools. The initial performance of each major detector subsystem is reviewed. We conclude with some preliminary analysis results and projections.

For an overview of the physics motivation and experimental challenges involved in measuring CP violation in the B system, we refer the reader to the lectures presented by Pat Burchat in these proceedings. We will assume that the reader of this report has a basic understanding of experimental high energy physics.

1 The PEP-II asymmetric B factory

The PEP-II asymmetric B factory resides at the Stanford Linear Accelerator Center (SLAC) in Menlo Park, California. The high design luminosity of 3×10^{33} cm^{-2} s^{-1} is achieved through high currents and strong focusing. A Snowmass year (10^7 s) of running at the design luminosity will yield 30 million B meson pairs, which meets the high statistics requirement for CP asymmetry measurements. The center-of-mass system is boosted in the lab ($\beta\gamma = 0.56$) through unequal beam energies in order to have an observable difference in the flight length of the two B hadrons ($\langle \delta z \rangle \approx 250$ μm), and thus an observable δt.

Commissioning of the high energy ring (HER) of the PEP-II machine began in May of '97. In March of '99, commissioning was put on hold to install the BaBar detector. By this point, PEP-II had already achieved a luminosity of 5.2×10^{32} cm^{-2} s^{-1} with 786 bunches. First collisions were recorded with the BaBar detector in May of '99, and PEP-II achieved a then world record luminosity of 1.4×10^{33} cm^{-2} s^{-1} in November of '99. The current PEP-II record is 1.95×10^{33} cm^{-2} s^{-1}. Figure 1 shows the integrated and daily luminosity history of PEP-II and the BaBar experiment. The inactive period near October '99 was a planned shutdown to install the remainder of

Work supported by the Department of Energy contract DE-AC02-76SF00515
SLAC, Stanford University, Stanford, CA 94309

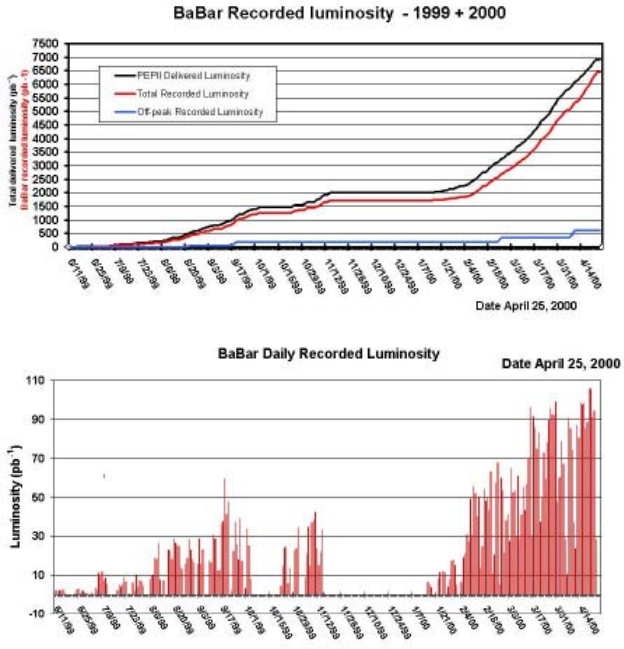

Figure 1. Integrated and daily luminosity history of PEP-II and the BaBar experiment.

the quartz bars for the DIRC particle ID system. The longer inactive period starting in November '99 was due to a PEP-II vacuum leak. BaBar has logged 6.5 fb^{-1} of data and now routinely records 100 pb^{-1} in one day.

2 Performance of the BaBar detector

The BaBar detector has a fairly standard collider-detector design [1]. At the center of the detector lies the silicon vertex tracker (SVT) which is a 5-layer, double-sided Si device designed to have a δz resolution better than 120 μm. The SVT is a stand-alone tracker, capable of reconstructing tracks down to a p_T of 60 MeV. The radial region from 23.6 cm to 81 cm is occupied by the drift chamber (DCH), which has 10 super layers with 4 cells per super layer. The super layers alternate between axial, U stereo, and V stereo. Outside the DCH lies the detector of internally reflected Čerenkov radiation (DIRC), which is a powerful particle identification tool unique to the BaBar experi-

ment. Outside the DIRC lies the CsI(Tl) electromagnetic calorimeter (EMC). The superconducting solenoid flux return is instrumented with resistive plate chambers (RPCs) for muon and neutral hadron identification. BaBar has a two-level trigger, which can operate at output rates of 2 KHz and 100 Hz for the first and second levels respectively. In the following subsections, we will describe the initial performance of the detector subsystems in more detail.

2.1 The silicon vertex tracker

The measured performance of the SVT is consistent with the design specifications. The electronic noise ranges from 800 to 1600 electrons which is well below the signal from a minimum-ionizing particle (about 22000 electrons at normal incidence). Although the PEP-II backgrounds are a bit larger than expected, we see no signs of serious radiation damage. For example, we see less than 10 dead channels due to radiation-induced p-stop shorts out of a total of 152K channels. Figure 2 shows the layer 1 hit resolution as measured in data compared to the Monte Carlo simulation. For tracks at normal incidence with the silicon, the hit resolution is about 12 μm in both the data and Monte Carlo.

The SVT is mounted on the PEP-II B1 dipole permanent magnets and can move with respect to the DCH by as much as 100 μm in a diurnal pattern. In order to maintain our desired resolution, we globally align the SVT with respect to the DCH after every run as a rolling calibration.

2.2 The drift chamber

The drift chamber momentum resolution has been measured with di-muon events to be $dp_t/p_t = 2.9\ \% \times p_t$ which is consistent with the design specification. Figure 2 shows the DCH hit resolution as a function of position within the cell. The hit resolution ranges from 100 to 200 μm with an average value of 125 μm, which exceeds the design specification of 140 μm. The DCH dE/dx resolution was measured to be 7.5% with Bhabha events. We hope to achieve the design specification of 7% with further corrections.

2.3 Integrated tracking performance

A good measure of the integrated tracking performance comes from mass resolutions. Figure 3 shows the mass resolution for $D^0 \to K^-\pi^+$ to be 8.8$\pm$1.7 MeV/c^2. The resolution for the narrow core of the $D^{*+} - D^0$ mass difference is 243 ± 7 KeV/c^2. Figure 4 shows the impact parameter resolution, in the xy and rz planes, as a function of transverse momentum as measured with

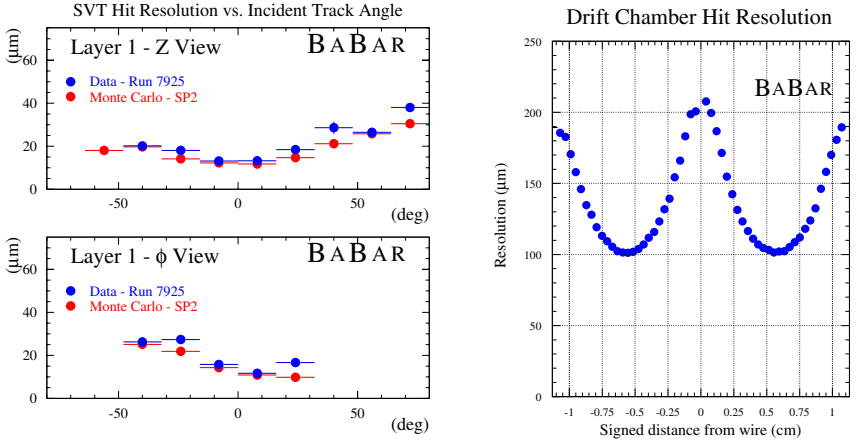

Figure 2. Layer 1 SVT hit resolution as a function of angle of incidence into the silicon and DCH hit resolution as a function of position within the cell.

multi-hadron events. The asymptotic value at high momentum, for both the xy and rz planes, is about 40 μm, which is consistent with an independent measurement with di-muon events at high momentum.

2.4 The detector of internally reflected Čerenkov radiation

The detector of internally reflected Čerenkov radiation (DIRC) is a powerful particle identification tool that is unique to the BaBar experiment. Čerenkov photons generated in an array of quartz bars that surround the outside of the drift chamber propagate through internal reflections to the end of the detector where they expand in a large water tank and are detected with an array of phototubes. The Čerenkov angle is measured and translates into the particle velocity, which can be used to infer the particle mass with the momentum measurement from the tracking system.

The quartz bars for the DIRC were technically very difficult to produce in large quantities. A typical photon travels 6 - 10 m within the quartz with about 300 reflections, so the bars need to have an extremely good polish (surface RMS of 5 - 10 Å) with sharp edges. Due to these technical challenges, a significant fraction of the bars were delivered 18 months late with a serious cost overrun.

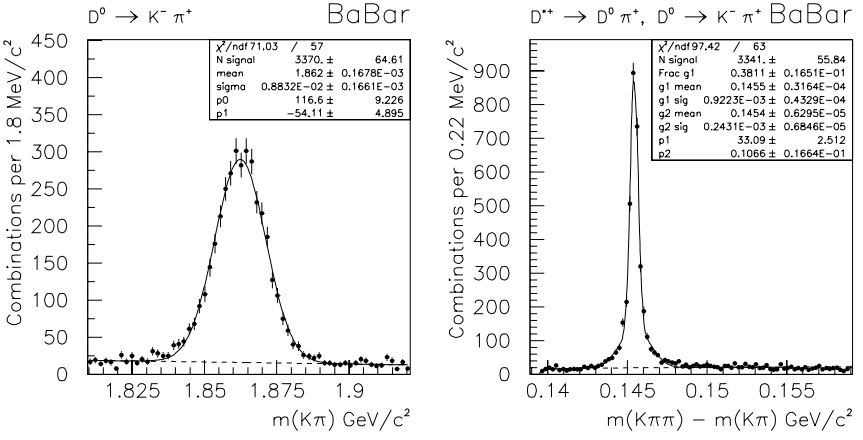

Figure 3. D^0 and $D^{*+} - D^0$ mass resolution.

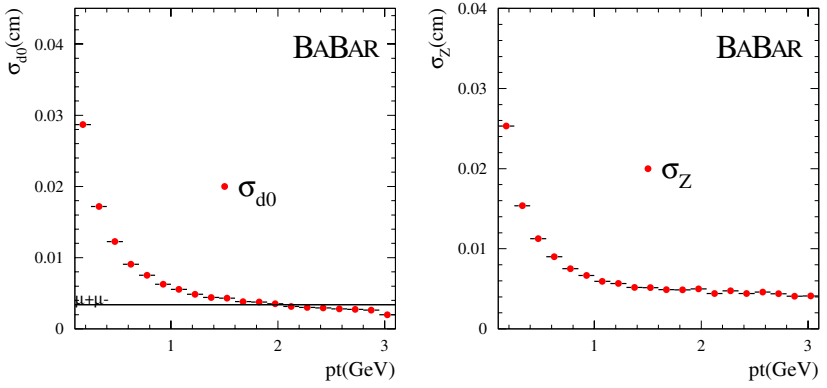

Figure 4. Impact parameter resolution as a function of transverse momentum.

We have measured the Čerenkov angle resolution to be 3.0 mrad with Bhabha events. To give the reader an idea of the necessary resolution, the π-K Čerenkov angle difference at 4.0 GeV/c is 6.4 mrad. We would like

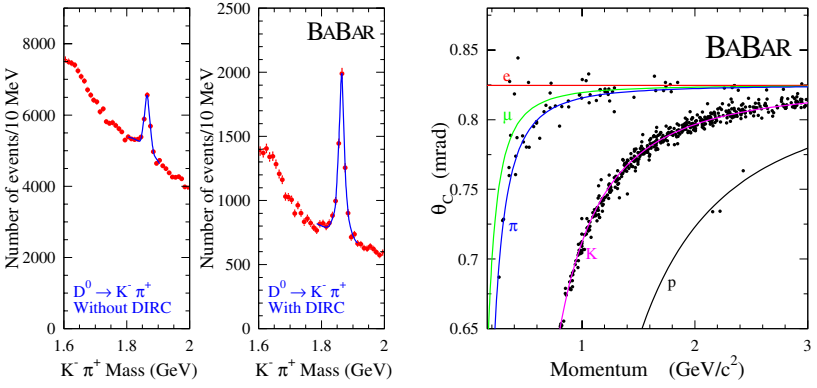

Figure 5. The enhancement in the $D^0 \to K^-\pi^+$ signal due to DIRC K identification and the measured Čerenkov angle as a function of momentum for kaons kinematically identified with $D^0 \to K^-\pi^+$.

to eventually achieve a resolution of 2 mrad, since good π-K separation is required at high momentum for the CP Eigenstate $B^0 \to \pi^+\pi^-$. Figure 5 shows the enhancement in the $D^0 \to K^-\pi^+$ signal when the kaon Čerenkov angle is required to be within 6 mrad (2 σ) of the expected value for a kaon. The efficiency is about 70-80% with a rejection factor of about 5. Figure 5 also shows the Čerenkov angle as a function of momentum for kaons that have been kinematically tagged with the decay chain $D^{*+} \to D^0\pi^+$, $D^0 \to K^-\pi^+$. The combinatoric background from the kinematic selection was about 15%.

2.5 The electromagnetic calorimeter

We have measured the resolution on the ratio of the observed energy to the expected energy with Bhabha electrons to be about 2%, which is consistent with the Monte Carlo simulation. Figure 6 shows the reconstructed $\pi^0 \to \gamma\gamma$ mass distribution from data, where the minimum γ energy is 30 MeV and the minimum π^0 energy is 300 MeV. The mass is consistent with the world average and the resolution is 7.4 MeV/c^2.

2.6 The instrumented flux return

We initially had problems in the instrumented flux return (IFR) with high currents in the RPCs due to the iron warming up, especially in the sum-

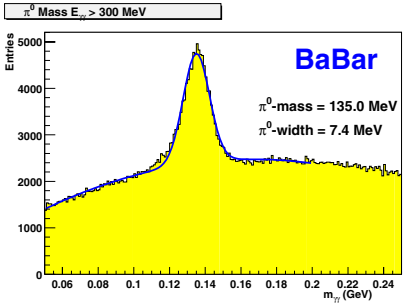

Figure 6. Reconstructed $\pi^0 \to \gamma\gamma$ with a minimum γ energy of 30 MeV and a minimum π^0 energy of 300 MeV.

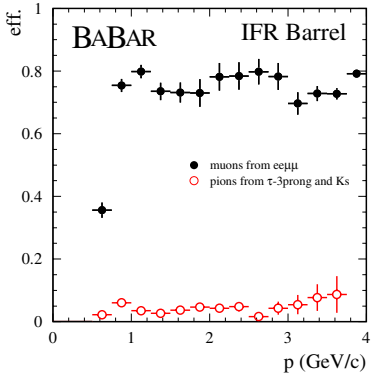

Figure 7. The instrumented flux return muon identification efficiency and pion misidentification fraction as a function of momentum.

mer. Many RPCs were temporarily disconnected before water cooling was installed on the flux return steel. Figure 7 shows the measured IFR muon identification efficiency and the pion misidentification rate as a function of momentum. Above 1 GeV/c, the muon ID efficiency is about 75%. The pion misidentification fraction is about 5%.

3 Demonstration of physics capability

The most theoretically clean and experimentally straight-forward CP asymmetry measurement comes from the decay $B^0 \to J/\psi K^0_s$, which gives $\sin(2\beta)$, where β is one of the angles of the Unitarity Triangle. Other experiments have already investigated CP violation with this mode [3]. BaBar plans to make a preliminary measurement of $\sin(2\beta)$ this summer using an integrated luminosity of about 10 fb^{-1}.

Figure 8 shows the inclusive J/ψ signal in the $\mu^+\mu^-$ and e^+e^- channels for an integrated luminosity of about 1.9 fb^{-1}. Figure 9 shows the beam-constrained mass distributions for $B^+ \to J/\psi K^+$ and $B^0 \to J/\psi K^0_s$, $K^0_s \to \pi^+\pi^-$ for an integrated luminosity of about 1.9 fb^{-1}. The yields are 109 ± 11 and 28 ± 5 for the $J/\psi K^+$ and $J/\psi K^0_s$ modes respectively, which are consistent with expectations.

A first step towards measuring a proper time dependent CP asymmetry is to measure the B^0 mixing frequency Δm_d through the proper time dependence of the flavor oscillations. The charge of the lepton from semileptonic B decay has the same sign as the b quark charge, so δm_d can be measured by following the number of same-sign and opposite-sign di-lepton events as a function of the longitudinal separation between the B decay vertices (δz). Figure 10 shows the dilepton asymmetry as a function of δz for selected events from 3 fb^{-1} along with the result of a fit for δm_d. The fitted value of δm_d is compatible with the world average and the statistical error is about 4%, which is the precision of the '98 world average [2].

BaBar expects to have recorded an integrated on-resonance luminosity of at least 10 fb^{-1} with the full detector by the end of August, 2000. With such a data set, the expected statistical precision of a measurement of $\sin(2\beta)$ with $B^0 \to J/\psi\ K^0_s$ is 0.25.

References

1. BaBar Technical Design Report, SLAC-R-457 (1995).
2. C. Caso et al. (PDG) Eur. Phys. J. **C3** (1998) 1.
3. T. Affolder *et al.* (CDF) Phys. Rev. D **61**, 072005 (2000).
   K. Ackerstaff *et al.* (OPAL) Eur. Phys. J. **C5** (1998) 379-388.
   Also see contributions by G. Apollinari and Andrew Halley in these proceedings.

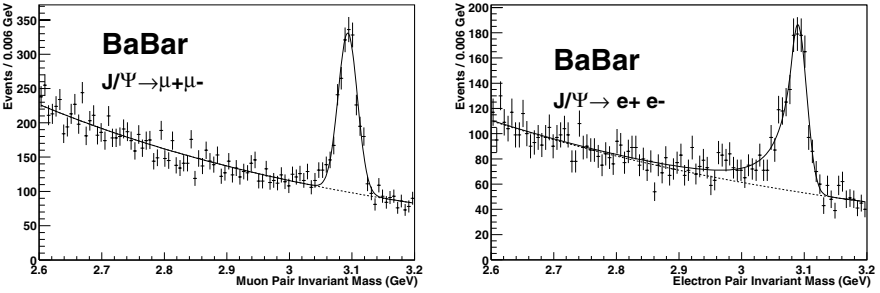

Figure 8. Invariant dilepton mass for the inclusive J/ψ signals in the $\mu^+\mu^-$ and e^+e^- channels.

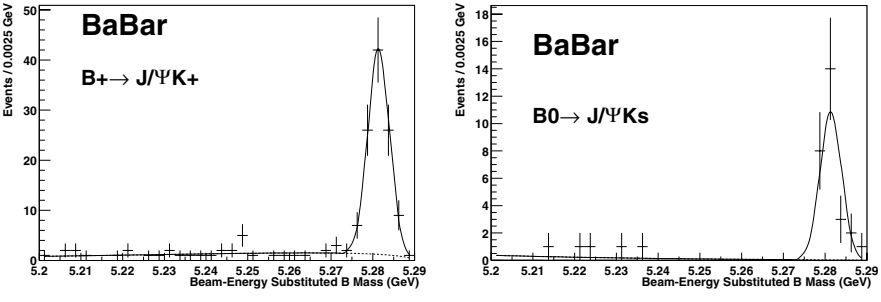

Figure 9. Invariant mass distributions for $B^+ \to J/\psi K^+$ and $B^0 \to J/\psi K_s^0$, $K_s^0 \to \pi^+\pi^-$.

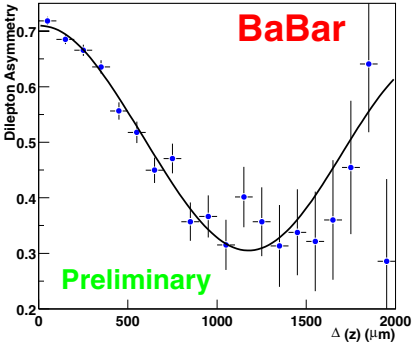

Figure 10. The di-lepton asymmetry as a function of δz for selected events. The curve represents the result of a fit for the mixing parameter δm_d.